Diiron Oxadithiolate Type Models for the Active Site of Iron-Only Hydrogenases and Biomimetic Hydrogen Evolution Catalyzed by Fe 2 (μ-SCH 2 OCH 2 S-μ)(CO) 6

ARTICLE *in* ORGANOMETALLICS · DECEMBER 2005

Impact Factor: 4.13 · DOI: 10.1021/om0507373

7 AUTHORS, INCLUDING:

Zhi-Yong Yang
Utah State University
23 PUBLICATIONS **675** CITATIONS

SEE PROFILE

Diiron Oxadithiolate Type Models for the Active Site of Iron-Only Hydrogenases and Biomimetic Hydrogen Evolution Catalyzed by $Fe_2(\mu\text{-}SCH_2OCH_2S\text{-}\mu)(CO)_6$

Li-Cheng Song,* Zhi-Yong Yang, Hong-Zhu Bian, Yang Liu, Hu-Ting Wang, Xu-Feng Liu, and Qing-Mei Hu

State Key Laboratory of Elemento-Organic Chemistry, Department of Chemistry, Nankai University, Tianjin 300071, People's Republic of China

Received August 26, 2005

The biomimetic chemistry of single and double oxadithiolatodiiron-containing model compounds for the active site of Fe-only hydrogenases (FeHases) has been systematically studied. The simplest such model, $Fe_2(\mu\text{-}SCH_2OCH_2S\text{-}\mu)(CO)_6$ (**1**), was prepared by reaction of $(\mu\text{-}S_2)Fe_2(CO)_6$ with 2 equiv of Et_3BHLi followed by direct treatment with excess $(ClCH_2)_2O$ or by successive treatment with 2 equiv of CF_3CO_2H and excess $(ClCH_2)_2O$ in the presence of Et_3N. Further reaction of **1** with 1 equiv of Me_3NO in MeCN at room temperature followed by treatment of the intermediate $Fe_2(\mu\text{-}SCH_2OCH_2S\text{-}\mu)(CO)_5L$ (L = MeCN or Me_3N) with 1 equiv of Et_4NCN, PPh_3, or $Cp(CO)_2FeSPh$ gave the single models $Fe_2(\mu\text{-}SCH_2OCH_2S\text{-}\mu)(CO)_5L_a$ (**2**, L_a = (CN)(Et_4N); **3**, PPh_3; **4**, $Cp(CO)_2FeSPh$) in 62−93% yields, whereas the in situ treatment of the intermediate $Fe_2(\mu\text{-}SCH_2OCH_2S\text{-}\mu)(CO)_5L$ with 0.5 equiv of 1,4-$(CN)_2C_6H_4$, $(\eta^5\text{-}Ph_2PC_5H_4)_2Fe$ (dppf), or $(\eta^5\text{-}Ph_2PC_5H_4)_2Ru$ (dppr) afforded the double models $[Fe_2(\mu\text{-}SCH_2OCH_2S\text{-}\mu)(CO)_5]_2L_b$ (**5**, L_b = 1,4-$(CN)_2C_6H_4$; **6**, dppf; **7**, dppr) in 57−90% yields. However, in contrast to **5**−**7**, the double models $[Fe_2(\mu\text{-}SCH_2OCH_2S\text{-}\mu)(CO)_n]_2L_c$ (**8**, $n = 5$, L_c = $(Ph_2PCH_2CH_2OCH_2)_2$; **9**, $n = 4$, L_c = $[(Ph_2PCH_2)_2NCH_2]_2$) could be prepared by direct reaction of **1** in toluene at reflux with 0.5 equiv of diphosphine $(Ph_2PCH_2CH_2OCH_2)_2$ and tetraphosphine $[(Ph_2PCH_2)_2NCH_2]_2$ in 86% and 56% yields, respectively. **1**−**9** were characterized by elemental analysis and spectroscopy, and particularly for **1**, **2**, and **4**−**9** by X-ray diffraction analysis. The structural features of some model compounds are compared with those of the active site of FeHases. While the cyclic voltammetric behavior of **1** and **5** was studied, **1** was found to be a catalyst for proton reduction of acetic acid to give hydrogen under the corresponding electrochemical conditions. An EECC mechanism for such electrocatalytic H_2 production is preliminarily suggested.

Introduction

Hydrogenases are highly efficient enzymes that catalyze both the reduction of protons and the oxidation of hydrogen in a variety of microorganisms.[1] Among such enzymes the Fe-only hydrogenases (FeHases) have recently received considerable attention because of their unusual structures and particularly their unique function for production of hydrogen, an alternative "clean" energy source.[2] The X-ray crystallographic[3−6] and IR spectroscopic[7−9] studies have revealed that the active site of FeHases, so-called H-cluster,[10] consists of a butterfly Fe_2S_2 subcluster that bears three unusual ligands, CO, CN^-, and Cys-S-Fe_4S_4, and a less defined three-light-atom linker possibly composed of carbon as in a 1,3-propanedithiolate bridge or any combination of C, N, and O atoms[5,11] bridged between two S atoms of the butterfly Fe_2S_2 subsite (Figure 1).

The structural studies concerning the active site of FeHases have greatly promoted the designed synthesis of model compounds for the active site that can perform the catalytic function similar to those in the natural systems.[1,2] To date, numerous models for the active diiron subsite have been synthesized, such as diiron propanedithiolate (PDT) derivatives,[12−15] diiron aza-

* To whom correspondence should be addressed. Fax: 0086-22-23504853. E-mail: lcsong@nankai.edu.cn.

(1) (a) Adams, M. W. W.; Stiefel, E. I. *Science* **1998**, *282*, 1842. (b) Cammack, R. *Nature* **1999**, *397*, 214.
(2) (a) Darensbourg, M. Y.; Lyon, E. J.; Zhao, X.; Georgakaki, I. P. *PNAS* **2003**, *100*, 3683. (b) Evans, D. J.; Pickett, C. *J. Chem. Soc. Rev.* **2003**, *32*, 268. (c) Alper, J. *Science* **2003**, *299*, 1686.
(3) Peters, J. W.; Lanzilotta, W. N.; Lemon, B. J.; Seefeldt, L. C. *Science* **1998**, *282*, 1853.
(4) Nicolet, Y.; Piras, C.; Legrand, P.; Hatchikian, E. C.; Fontecilla-Camps, J. C. *Structure* **1999**, *7*, 13.
(5) Nicolet, Y.; De Lacey, A. L.; Vernède, X.; Fernandez, V. M.; Hatchikian, E. C.; Fontecilla-Camps, J. C. *J. Am. Chem. Soc.* **2001**, *123*, 1596.
(6) Lemon, B. J.; Peters, J. W. *Biochemistry* **1999**, *38*, 12969.
(7) Pierik, A. J.; Hulstein, M.; Hagen, W. R.; Albracht, S. P. J. *Eur. J. Biochem.* **1998**, *258*, 572.
(8) De Lacey, A. L.; Stadler, C.; Cavazza, C.; Hatchikian, E. C.; Fernandez, V. M. *J. Am. Chem. Soc.* **2000**, *122*, 11232.
(9) Chen, Z.; Lemon, B. J.; Huang, S.; Swartz, D. J.; Peters, J. W.; Bagley, K. A. *Biochemistry* **2002**, *41*, 2036.
(10) Adams, M. W. W. *Biochim. Biophys. Acta* **1990**, *1020*, 115.
(11) Nicolet, Y.; Lemon, B. J.; Fontecilla-Camps, J. C.; Peters, J. W. *Trends Biochem. Sci*. **2000**, *25*, 138.
(12) Zhao, X.; Georgakaki, I. P.; Miller, M. L.; Yarbrough, J. C.; Darensbourg, M. Y. *J. Am. Chem. Soc.* **2001**, *123*, 9710.
(13) Gloaguen, F.; Lawrence, J. D.; Schmidt, M.; Wilson, S. R.; Rauchfuss, T. B. *J. Am. Chem. Soc*. **2001**, *123*, 12518.

10.1021/om0507373 CCC: $30.25
Publication on Web 11/01/2005

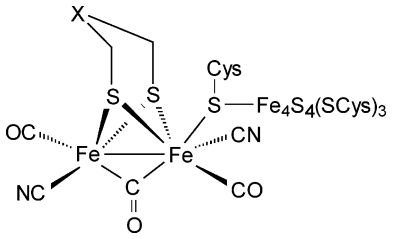

Figure 1. Composite structure for the active site based on the crystal structures of FeHases (X = CH_2, NH, or O).

dithiolate (ADT) derivatives,[16−18] and the very recently reported diiron PDT derivatives with a cubic Fe_4S_4 cluster.[19] In a recent communication we preliminarily reported several diiron oxadithiolate (ODT) type model compounds.[20] Now, in this paper we will describe the detailed synthesis and structural characterization regarding those briefly reported compounds and some others that are new, containing either a single or a double diiron oxadithiolate moiety. In addition,we will also report the electrochemical properties associated with two representative compounds and the biomimetic hydrogen evolution catalyzed by the parent compound of these described ODT type models.

Results and Discussion

Synthesis and Characterization of Model Compounds Containing a Single Diiron Oxadithiolate Moiety. The parent compound of this series is $Fe_2(\mu\text{-}SCH_2OCH_2S\text{-}\mu)(CO)_6$ (**1**), which was prepared by reaction of $(\mu\text{-}S_2)Fe_2(CO)_6$ with 2 equiv of $LiBEt_3H$ in THF at −78 °C, followed by treatment of the intermediate $(\mu\text{-}LiS)_2Fe_2(CO)_6$[21a] with excess bis(chloromethyl) ether. This compound could also be prepared by treatment of the intermediate $(\mu\text{-}LiS)_2Fe_2(CO)_6$ with ca. 2 equiv of CF_3CO_2H and subsequent treatment of the intermediate $(\mu\text{-}HS)_2Fe_2(CO)_6$[21b] with excess $(ClCH_2)_2O$ in the presence of Et_3N (Scheme 1). In fact, **1** had been prepared before our synthesis by another method and characterized by spectroscopy.[17] Our solid IR spectrum of **1** showed four strong bands in the range 2077−1989 cm^{-1}, and the reported solution IR spectrum[17] displayed five strong bands in the region 2079−1987 cm^{-1}, all assignable to its terminal carbonyls. Both the above-mentioned IR spectra, except some minor differences such as in band number, are very similar to the solution IR spectrum of its PDT analogue $Fe_2(\mu\text{-}SCH_2CH_2CH_2S\text{-}\mu)(CO)_6$, which showed three strong bands from 2072 to 1993 cm^{-1} for its terminal carbonyl ligands.[22] To confirm the structure of **1** and to get its detailed structural information, we carried out the X-ray crystallographic study of **1**. Figure 2 shows its ORTEP drawing, while Table 1 lists the selected bond lengths and angles. As shown in Figure 2, complex **1** is indeed composed of an oxadithiolate ligand bridged between two iron atoms each with three terminal CO ligands. The coordination geometry of the iron atoms in **1**, similar to its PDT analogue $Fe_2(\mu\text{-}SCH_2CH_2CH_2S\text{-}\mu)$-

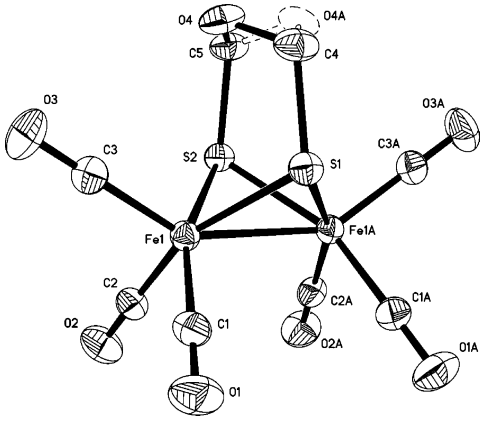

Figure 2. ORTEP view of **1** with 30% probability level ellipsoids.

Scheme 1

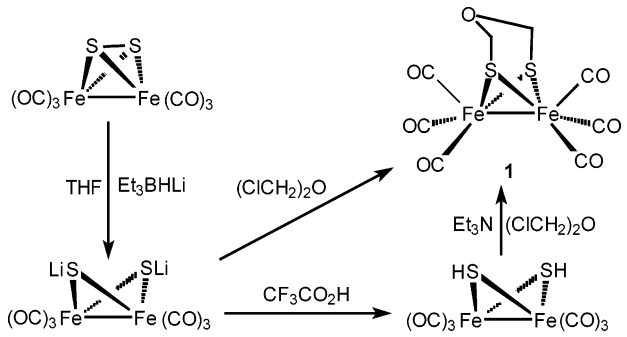

Table 1. Selected Bond Lengths (Å) and Angles (deg) for 1, 2, and 4

		1	
Fe(1)−S(1)	2.2526(10)	1Fe(1)−Fe(1A)	2.5113(13)
Fe(1)−S(2)	2.2526(11)	Fe(1A)−S(2)	2.2526(11)
S(1)−C(4)	1.828(4)	C(5)−O(4)	1.385(5)
S(2)−C(5)	1.836(4)	C(4)−O(4)	1.413(5)
S(1)−Fe(1)−S(2)	84.97(4)	C(4)−S(1)−Fe(1)	110.14(11)
S(1)−Fe(1)−Fe(1A)	56.12(2)	C(5)−O(4)−C(4)	135.0(3)
C(4)−S(1)−Fe(1A)	110.14(11)	O(4)−C(4)−S(1)	115.7(3)
Fe(1)−S(1)−Fe(1A)	67.76(4)	O(4)−C(5)−S(2)	115.6(3)
		2	
Fe(1)−S(1)	2.2640(16)	Fe(2)−S(2)	2.2386(17)
Fe(1)−S(2)	2.2699(18)	C(7)−O(7)	1.415(7)
S(1)−C(8)	1.840(6)	Fe(1)−Fe(2)	2.5121(13)
Fe(2)−S(1)	2.2461(17)	N(1)−C(6)	1.149(6)
S(1)−Fe(2)−Fe(1)	56.49(4)	Fe(2)−S(1)−Fe(1)	67.70(5)
S(2)−Fe(2)−S(1)	85.49(7)	N(1)−C(6)−Fe(2)	176.5(5)
S(2)−Fe(2)−Fe(1)	56.73(5)	C(8)−O(7)−C(7)	112.6(5)
S(1)−Fe(1)−S(2)	84.35(6)	S(2)−Fe(1)−Fe(2)	55.55(4)
		4	
Fe(2)−S(2)	2.2556(14)	Fe(2)−Fe(3)	2.5026(14)
Fe(2)−S(1)	2.2998(17)	Fe(3)−S(3)	2.2687(15)
S(2)−C(8)	1.809(5)	C(8)−O(8)	1.404(5)
Fe(1)−S(1)	2.3016(14)	Fe(3)−S(2)	2.2670(15)
S(1)−Fe(2)−S(2)	103.03(4)	Fe(3)−S(3)−Fe(2)	66.72(5)
S(2)−Fe(2)−Fe(3)	56.62(3)	S(2)−Fe(2)−S(3)	84.67(6)
S(1)−Fe(2)−Fe(3)	145.02(4)	S(3)−Fe(2)−Fe(3)	56.38(4)
S(2)−Fe(3)−S(3)	84.71(6)	S(3)−Fe(3)−Fe(2)	56.90(4)

(14) (c) Lyon, E. J.; Georgakaki, I. P.; Reibenspies, J. H.; Darensbourg, M. Y. *J. Am. Chem. Soc.* **2001**, *123*, 3268.
(15) Razavet, M.; Davies, S. C.; Hughes, D. L.; Barclay, J. E.; Evans, D. J.; Fairhurst, S. A.; Liu, X.; Pickett, C. J. *Dalton Trans.* **2003**, 586.
(16) Lawrence, J. D.; Li, H.; Rauchfuss, T. B.; Bénard, M.; Rohmer, M.-M. *Angew. Chem., Int. Ed.* **2001**, *40*, 1768.
(17) Li, H.; Rauchfuss, T. B. *J. Am. Chem. Soc.* **2002**, *124*, 726.
(18) Ott, S.; Kritikos, M.; Åkermark, B.; Sun, L. *Angew. Chem., Int. Ed.* **2003**, *42*, 3285.
(19) Tard, C.; Liu, X.; Ibrahim, S. K.; Bruschi, M.; De Gioia, L.; Davies, S. C.; Yang, X.; Wang, L.-S.; Sawers, G.; Pickett, C. J. *Nature* **2005**, *433*, 610.
(20) Song, L.-C.; Yang, Z.-Y.; Bian, H.-Z.; Hu, Q.-M. *Organometallics* **2004**, *23*, 3082.
(21) (a) Seyferth, D.; Henderson, R. S.; Song, L.-C. *Organometallics* **1982**, *1*, 125. (b) Seyferth, D.; Henderson, R. S.; Song, L.-C. *J. Organomet. Chem.* **1980**, *192*, C1.

Scheme 2

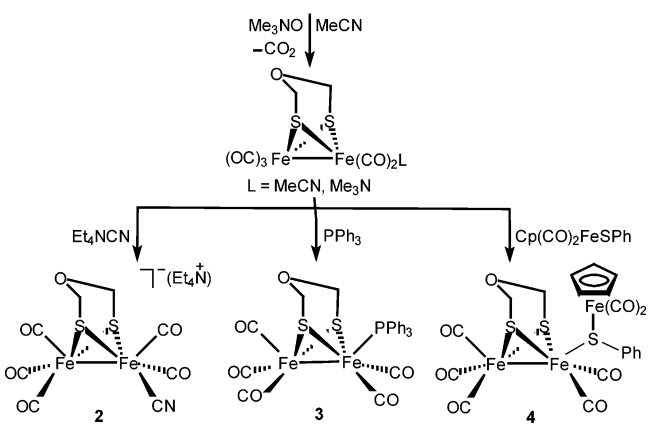

$(CO)_6$,[22] is roughly square pyramidal with each iron atom being displaced by about 0.38 Å from the pyramidal base toward the apical direction. The Fe−Fe bond length in **1** is equal to 2.5113(13) Å, ca. 0.1 Å shorter than those reported for the oxidized state diiron subsite in the enzyme structures (2.62 and 2.60 Å)[3,4] and only 0.04 Å shorter than that in the reduced state diiron subsite of the enzyme structure (2.55 Å).[5] In addition, as can be seen in Figure 2, the bridgehead oxygen atom is disordered (50%), which agrees very well with the solution ^{1}H NMR spectrum of **1** showing only one singlet at 4.21 ppm.

Interestingly, it was found that the ODT-type model compounds with a single diiron oxadithiolate moiety can be prepared from parent compound **1** in good to excellent yields. For instance, when **1** was reacted with 1 equiv of decarbonylation agent $Me_3NO{\cdot}2H_2O$ in MeCN at room temperature followed by treatment of the intermediate $Fe_2(\mu\text{-}SCH_2OCH_2S\text{-}\mu)(CO)_5L$ (L = MeCN or Me_3N)[13] with 1 equiv of Et_4NCN, PPh_3, or $Cp(CO)_2$FeSPh, the corresponding single ODT type model compounds $[Fe_2(\mu\text{-}SCH_2OCH_2S\text{-}\mu)(CO)_5(CN)](Et_4N)$ (**2**), $Fe_2(\mu\text{-}SCH_2OCH_2S\text{-}\mu)(CO)_5(PPh_3)$ (**3**), and $[Fe_2(\mu\text{-}SCH_2OCH_2S\text{-}\mu)(CO)_5][Cp(CO)_2FeSPh]$ (**4**) were produced in 62%, 93%, and 72% yields, respectively (Scheme 2).

Compounds **2**−**4** have been characterized by elemental analysis, IR and ^{1}H NMR spectroscopy. The IR spectra of **2**−**4** showed several absorption bands in the range 2041−1907 cm^{-1} for their terminal carbonyls, which lie at much lower frequency relative to those (2077−1989 cm^{-1}) of parent compound **1**. This is obviously due to the increased strength of back-bonding between iron atoms and the attached carbonyls by CO substitution with the stronger electron-donating ligands CN^-, PPh_3, and $Cp(CO)_2$FeSPh. The ^{1}H NMR spectrum of **2** displayed a singlet at 4.09 ppm assigned to two magnetically identical protons in its methylene groups, whereas **3** and **4** exhibited two broad singlets at 4.2−3.3 ppm attributed to two magnetically different protons in their methylene groups.

The molecular structures of **2** and **4** were unambiguously confirmed by crystal X-ray diffraction analysis. While ORTEP views of **2** and **4** are presented in Figures 3 and 4, their selected bond lengths and angles are given in Table 1.

(22) Lyon, E. J.; Georgakaki, I. P.; Reibenspies, J. H.; Darensbourg, M. Y. *Angew. Chem., Int. Ed.* **1999**, *38*, 3178.

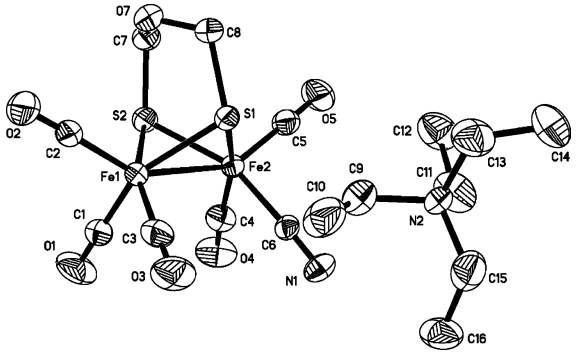

Figure 3. ORTEP view of **2** with 30% probability level ellipsoids.

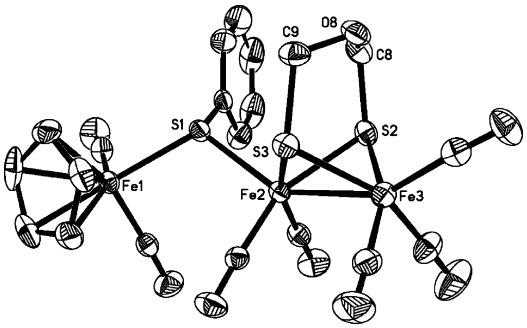

Figure 4. ORTEP view of **4** with 30% probability level ellipsoids.

Figure 3 shows that **2** is the $(Et_4N)^+$ salt of complex anion $[Fe_2(\mu\text{-}SCH_2OCH_2S\text{-}\mu)(CO)_5(CN)]^-$, in which the CN^- ligand occupies an equatorial coordination site of one Fe atom. This is in accordance with its position in the H-cluster of FeHases.[3−6] The fact that the distances between Fe(2) and its attached CO-carbon atoms are shorter than those around Fe(1) proves the increased strength of back-bonding between Fe(2) and C(4)O(4) or C(5)O(5) caused by coordination of the strong σ-donor ligand CN^-. In addition, the bridgehead oxygen atom in **2**, in contrast to that in parent complex **1**, is fixed completely opposite the Fe atom attached to the CN^- ligand, which could be attributed to the strong electrostatic repulsion between the negatively charged CN^- ligand and the electronegative O atom.

Figure 4 indicates that complex **4** contains a metallo-thioether ligand $Cp(CO)_2$FeSPh, which is coordinated via its S atom to one of the Fe atoms of the butterfly Fe_2S_2 cluster. Interestingly, this simple metallo-thioether seems to be a good ligand for mimicking to a certain degree the real, complicated metallo-thioether ligand Cys-S-Fe_4S_4,[3−6] since they are both coordinated to one of the Fe atoms of the butterfly Fe_2S_2 cluster through the S atom in their Fe-thioether structural units. While the metal−metal bond Fe(2)−Fe(3) is 2.5026(14) Å, the nonbonded metal−metal Fe(1)···Fe(2) distance is 3.866 Å. The bond lengths Fe(1)−S(1) (2.3016(14) Å) and Fe(2)−S(1) (2.2998(17) Å) are virtually the same, whereas the Fe−S bond lengths (2.2556(14)−2.2821(14) Å) in its butterfly cluster core are quite different. As can be seen intuitively in Figure 4, the bridgehead O atom points opposite the axially substituted metallo-thioether ligand, which is possibly in order to avoid the strong steric repulsion between the bulky ligand $Cp(CO)_2$FeSPh and the bridgehead O atom when it points to the bulky ligand.

Scheme 3

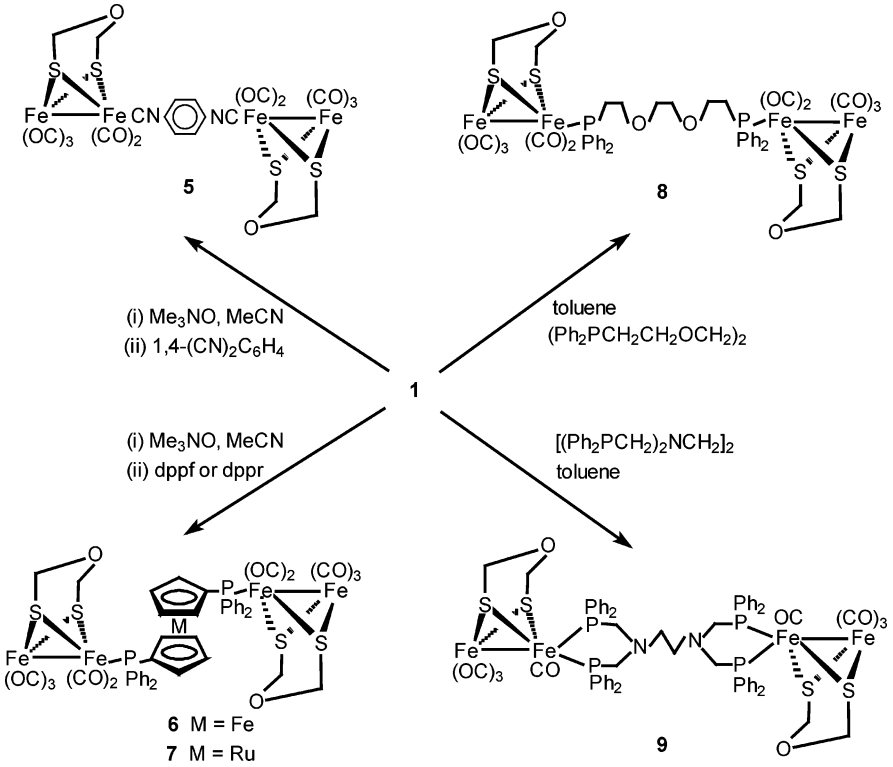

Unfortunately, the molecular structure of **3** has not been characterized so far by X-ray diffraction, due to lack of X-ray quality single crystals. However, it is believed that the PPh_3 ligand in **3** is most likely substituted axially at one of its two Fe atoms. This is because such an axially substituted pattern has been found in similar substituted complexes, such as the mono-PPh_3-substituted derivative (μ-cyclo-$C_6H_{11}S$)(μ-*n*-$C_5H_{11}S$)$Fe_2(CO)_5(PPh_3)$[23] and the bis-PPh_3-substituted complex (μ-*i*-C_3H_7S)(μ-$PhCH_2S$)$Fe_2(CO)_4(PPh_3)_2$.[24]

Synthesis and Characterization of Model Compounds Containing a Double-Diiron Oxadithiolate Moiety. Similar to the double-cubane $MoFe_3S_4$ model for the Mo/Fe cofactor of nitrogenases that has two active sites,[25] we further prepared a series of model compounds containing two diiron oxadithiolate active sites by reaction of parent compound **1** with 1 equiv of $Me_3NO{\cdot}2H_2O$ in MeCN at room temperature followed by treatment of the intemediate $Fe_2(\mu\text{-}SCH_2OCH_2S\text{-}\mu)(CO)_5L$ (L = MeCN or Me_3N)[13] with 0.5 equiv of 1,4-diisocyanobenzene, 1,1′-bis(diphenylphosphino)ferrocene (dppf), or 1,1′-bis(diphenylphosphino)ruthenocene (dppr), affording the corresponding double ODT type model compounds $[Fe_2(\mu\text{-}SCH_2OCH_2S\text{-}\mu)(CO)_5]_2[1,4\text{-}(CN)_2C_6H_4]$ (**5**), $[Fe_2(\mu\text{-}SCH_2OCH_2S\text{-}\mu)(CO)_5]_2[(\eta^5\text{-}Ph_2PC_5H_4)_2Fe]$ (**6**), and $[Fe_2(\mu\text{-}SCH_2OCH_2S\text{-}\mu)(CO)_5]_2[(\eta^5\text{-}Ph_2PC_5H_4)_2Ru]$ (**7**) in 57%, 90%, and 84% yields, respectively (Scheme 3). However, when **1** was directly reacted with 0.5 equiv of diphosphine ligand $(Ph_2PCH_2CH_2OCH_2)_2$ or tetraphosphine ligand $[(Ph_2PCH_2)_2NCH_2]_2$ in toluene at reflux, the corresponding double ODT type model compounds $[Fe_2(\mu\text{-}SCH_2OCH_2S\text{-}\mu)(CO)_5]_2(Ph_2PCH_2CH_2OCH_2)_2$ (**8**) and $[Fe_2(\mu\text{-}SCH_2OCH_2S\text{-}\mu)(CO)_4]_2[(Ph_2PCH_2)_2NCH_2]_2$ (**9**) were obtained in 86% and 56% yields, respectively (Scheme 3).

Compounds **5**−**9** have been fully characterized by elemental analysis, spectroscopy, and X-ray diffraction techniques. For example, the IR spectra of **5**−**9** displayed three absorption bands in the range 2047−1900 cm^{-1} for their terminal carbonyls. These bands are located at much lower frequency relative to those of parent compound **1** on the basis of the same reason for **2**−**4**. In addition, the ^1H NMR spectra of **5**−**9** showed the corresponding proton signals for their respective organic groups, whereas the ^{31}P NMR spectra of **6**−**9** exhibited one singlet at ca. 50 ppm for their identical P atoms in each of their bridging ligands.

The molecular structures of **5**−**9** have been unequivocally confirmed by X-ray diffraction methods. While ORTEP views of **5**−**9** are shown in Figures 5−9, selected bond lengths and angles are listed in Table 2.

It can be seen in Figure 5 that model compound **5** indeed consists of two diiron oxadithiolate moieties,

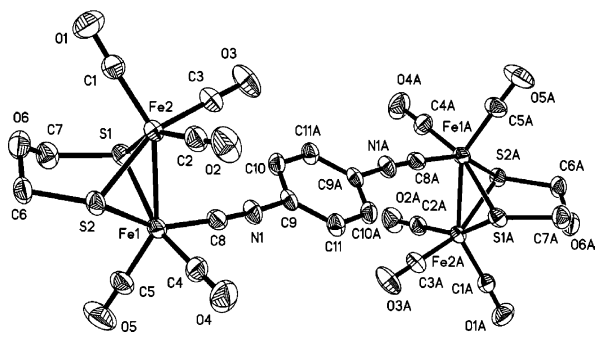

Figure 5. ORTEP view of **5** with 30% probability level ellipsoids.

(23) Song, L.-C.; Hu, Q.-M.; Wang, J.-T.; Lin, X.-Y.; Zheng, Q.-T.; Zhang, S.-D.; Shen, F.-L.; Wu, S. *Acta Chim. Sin.* **1986**, *44*, 558.
(24) Song, L.-C.; Hu, Q.-M.; Wang, R.-J.; Wang, H.-G. *Acta Chim. Sin.* **1988**, *46*, 984.
(25) Kovacs, J. A.; Bashkin, J. K.; Holm, R. H. *J. Am. Chem. Soc.* **1985**, *107*, 1784.

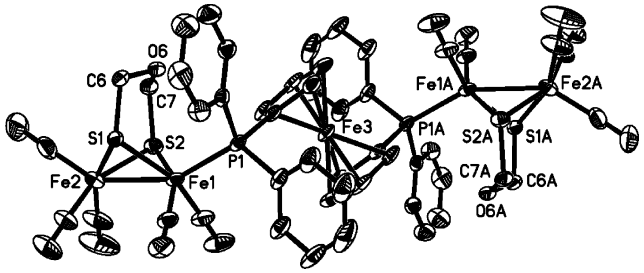

Figure 6. ORTEP view of **6** with 30% probability level ellipsoids.

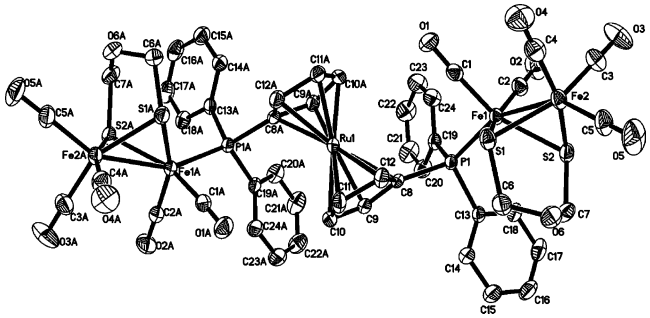

Figure 7. ORTEP view of **7** with 30% probability level ellipsoids.

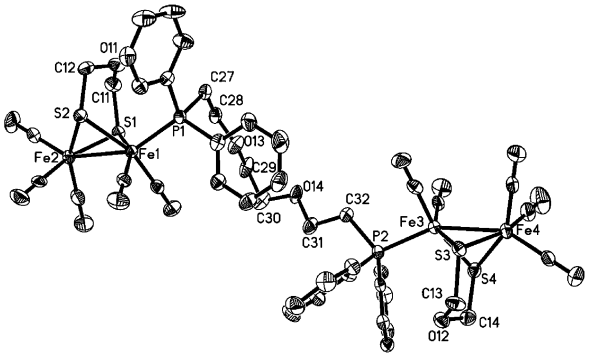

Figure 8. ORTEP view of **8** with 30% probability level ellipsoids.

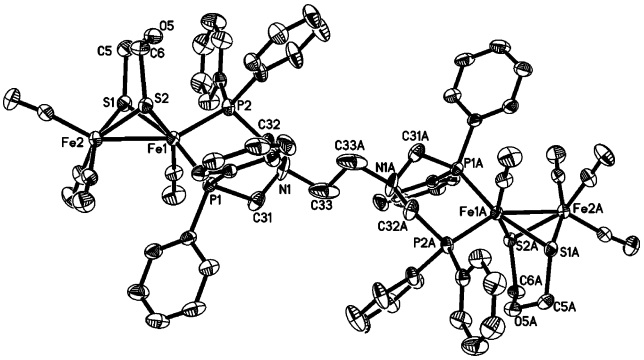

Figure 9. ORTEP view of **9** with 30% probability level ellipsoids.

which are joined together through an equatorially substituted 1,4-diisocyanobenzene ligand. This molecule is centrosymmetric. Both bridgedhead O atoms of the oxadithiolates point opposite the diisocyano ligand. This is probably due to the greater electrostatic repulsion between the electronegative diisocyano ligand (a stronger σ-donor than CO) and the electronegative O atoms when they point in the direction of the diisocyano ligand. The distance between Fe(1) or Fe(1A) and C atoms of the two isocyano groups is 1.840 (3) Å, which lies in the range 1.759−1.875 Å found for other isonitrile complexes.[26]

Table 2. Selected Bond Lengths (Å) and Angles (deg) for 5−9

		5	
Fe(1)−Fe(2)	2.4938(11)	Fe(1)−S(2)	2.2366(12)
Fe(1)−S(1)	2.2453(13)	Fe(2)−C(1)	1.777(4)
Fe(2)−S(1)	2.2551(12)	Fe(2)−S(2)	2.2490(12)
S(1)−Fe(1)−Fe(2)	56.54(3)	Fe(1)−S(1)−Fe(2)	67.30(4)
S(2)−Fe(1)−S(1)	84.90(4)	C(7)−O(6)−C(6)	112.9(3)
S(2)−Fe(1)−Fe(2)	56.46(4)	S(1)−Fe(2)−Fe(1)	56.16(4)
		6	
Fe(1)−S(1)	2.2612(19)	Fe(2)−S(2)	2.2571(19)
Fe(1)−S(2)	2.279(2)	S(1)−C(6)	1.830(6)
Fe(2)−S(1)	2.268(2)	O(6)−C(7)	1.405(7)
S(1)−Fe(1)−S(2)	83.97(7)	S(1)−Fe(2)−Fe(1)	55.72(5)
S(1)−Fe(1)−Fe(2)	55.96(6)	Fe(2)−S(2)−Fe(1)	68.20(6)
S(2)−Fe(1)−Fe(2)	55.50(5)	C(8)−P(1)−Fe(1)	117.9(2)
		7	
Fe(2)−Fe(1)	2.5383(11)	Fe(1)−S(2)	2.2716(15)
Fe(1)−S(1)	2.2543(15)	Fe(2)−S(2)	2.2689(17)
Fe(2)−S(1)	2.2559(16)	P(1)−C(8)	1.808(4)
P(1)−Fe(1)−S(1)	106.19(5)	S(2)−Fe(1)−Fe(2)	55.96(4)
S(1)−Fe(1)−S(2)	84.00(5)	S(1)−Fe(2)−S(2)	84.02(5)
S(1)−Fe(1)−Fe(2)	55.78(4)	S(1)−Fe(2)−Fe(1)	55.72(4)
		8	
Fe(2)−Fe(1)	2.512(2)	Fe(2)−S(1)	2.252(3)
Fe(1)−P(1)	2.242(3)	S(1)−C(11)	1.824(9)
Fe(1)−S(1)	2.256(3)	O(11)−C(12)	1.393(11)
P(1)−Fe(1)−S(1)	109.18(10)	S(2)−Fe(1)−S(1)	84.14(10)
P(1)−Fe(1)−Fe(2)	151.94(8)	S(2)−Fe(1)−Fe(2)	55.80(7)
S(1)−Fe(1)−Fe(2)	56.05(7)	S(1)−Fe(2)−Fe(1)	56.22(7)
		9	
Fe(1)−P(1)	2.2107(19)	O(5)−C(6)	1.398(8)
Fe(1)−S(2)	2.2673(18)	N(1)−C(31)	1.448(9)
Fe(2)−S(1)	2.266(2)	Fe(1)−Fe(2)	2.5363(14)
P(1)−Fe(1)−P(2)	92.89(7)	Fe(1)−S(1)−Fe(2)	68.13(5)
P(1)−Fe(1)−S(2)	93.82(7)	C(31)−P(1)−Fe(1)	113.1(2)
P(1)−Fe(1)−Fe(2)	111.63(6)	C(6)−O(5)−C(5)	113.1(5)

The double ODT type model compounds **6** and **7**, as shown in Figures 6 and 7, contain an organometallic diphosphine dppf or dppr ligand, which is axially coordinated to two iron atoms of the two diiron oxadithiolate structural units through two P atoms of the diphosphine ligand. Both structures are centrosymmetric. However, while in **6** the two bridgehead O atoms point in the direction of diphosphine dppf, the two O atoms in **7** are directed opposite diphosphine dppr. The bond lengths of Fe(1)−Fe(2) in **6** (2.5430(16) Å) and in **7** (2.5383(11) Å) are very close to those in the oxidized form (2.62 and 2.60 Å)[3,4] and the reduced form (2.55 Å)[5] of the enzymes.

Similar to **6** and **7**, the double ODT type model **8**, as shown in Figure 8, includes an ether chain-bridged diphosphine ligand $(Ph_2PCH_2CH_2OCH_2)_2$, which is axially bonded to two iron atoms of the two ODT moieties. It is particularly interesting that model compound **9** (Figure 9) contains a tetraphosphine ligand $[(Ph_2PCH_2)_2NCH_2]_2$, which is chelated to two iron atoms of each ODT moiety through an equatorial P−Fe bond and an

(26) (a) Lawrence, J. D.; Rauchfuss, T. B.; Wilson, S. R. *Inorg. Chem.* **2002**, *41*, 6193. (b) Lai, C.-H.; Lee, W.-Z.; Miller, M. L.; Reibenspies, J. H.; Darensbourg, D. J.; Darensbourg, M. Y. *J. Am. Chem. Soc.* **1998**, *120*, 10103. (c) Nehring, J. L.; Heinekey, D. M. *Inorg. Chem.* **2003**, *42*, 4288.

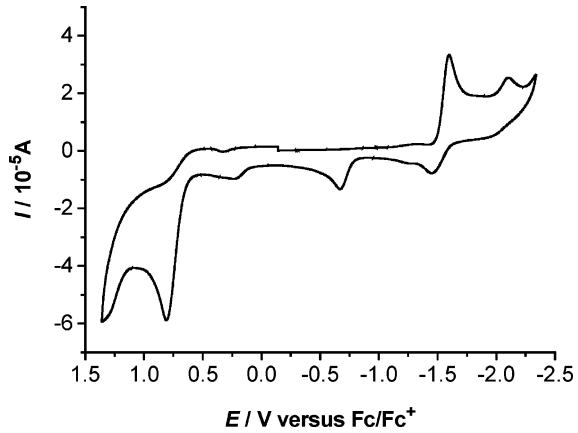

Figure 10. Cyclic voltammogram of **1** (1 mM) in 0.1 M n-Bu_4NPF_6/MeCN at a scan rate of 100 mV·s^{-1}.

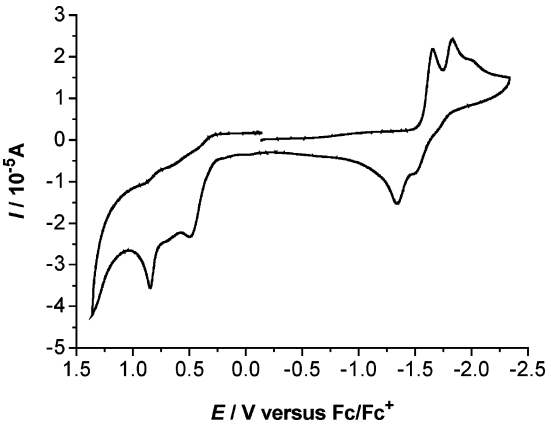

Figure 11. Cyclic voltammogram of **5** (1 mM) in 0.1 M n-Bu_4NPF_6/MeCN at a scan rate of 100 mV·s^{-1}.

axial P−Fe bond, respectively. In addition, this molecule is centrosymmetric and the two bridgehead O atoms are directed toward the tetraphosphine ligand.

Finally, it is worth pointing out that the bond lengths of Fe(1)−Fe(2) in **8** (2.512(2) Å) and **9** (2.5363(14) Å) are very close to those in **6** and **7**, as well as in the oxidized form and the reduced form of the enzymes (2.62, 2.60, and 2.55 Å, respectively).[3−5] In addition, the strong σ-donor nature of diphosphine and particularly tetraphosphine in **8** and **9** would make their Fe−Fe bonds more electron-rich and thus might facilitate protonation of the diiron subsite, the important step for the possible electrocatalytic proton reduction to dihydrogen.[27−31]

Electrochemistry of Model Compounds 1 and 5. Although the electrochemical properties of the PDT type[27−29] and ADT type[30,31] model compounds were previously reported, no such properties have been reported in the literature so far concerning the ODT type model compounds.

Now, we report the electrochemical properties of **1** and **5** as representatives of the single and double ODT type model compounds. The cyclic voltammograms of **1** and **5** are shown in Figures 10 and 11, respectively. Interestingly, as shown in Figure 10, the single model **1** displays three electrochemical events, which include one irreversible oxidation at +0.81 V, one quasi-reversible reduction at −1.59 V, and one irreversible reduction at − 2.10 V, respectively. The bulk electrolysis of **1** (0.022 mM) at − 1.80 V in MeCN demonstrated that the two reduction events are one-electron processes, which can be assigned to the $Fe^IFe^I + e^- \rightarrow Fe^0Fe^I$ and $Fe^0Fe^I + e^- \rightarrow Fe^0Fe^0$ couples. However, the oxidation process occurring at +0.81 V is a two-electron process, attributed to the $Fe^IFe^I \rightarrow Fe^{II}Fe^{II} + 2\ e^-$ couple, since its peak current is about twice as much as that of each of the one-electron reduction processes mentioned above. In addition, it is worth pointing out that in Figure 10 there are still two small irreversible oxidation peaks at −0.61 and + 0.23 V. These two oxidation peaks are probably due to some unknown species generated from decomposition of **1** during the course of cyclic voltammetric determination. In fact, such cyclic voltammetric behavior is similar to those exhibited by its PDT- and ADT-bridged analogues.[27−31]

As can be seen in Figure 11, the double model **5** shows two quasi-reversible reductions at −1.65 and −1.82 V, as well as two irreversible oxidations at +0.50 and +0.85 V, respectively. The potential difference between the two reductions of **5** is 0.17 V, which is much smaller than that (0.51 V) between the two reductions of **1**. Therefore, the two reductions of **5** should be assigned to the two sequential one-electron reduction events of the two iron atoms in the two diiron subsites. In addition, the two iron atoms in the two diiron subsites should be distant from the diisonitrile ligand since 1,4-diisocyanobenzene is a stronger electron-donating ligand than CO, namely, $Fe^IFe^I(CNC_6H_4) + e^- \rightarrow Fe^0Fe^I(CNC_6H_4)$ and $(C_6H_4NC)Fe^IFe^I + e^- \rightarrow (C_6H_4NC)Fe^IFe^0$. This is consistent with the first reduction peak of **5** being negatively shifted by −0.06 V and the second reduction peak negatively shifted by −0.23 V relative to the first reduction peak of **1**, respectively. Similarly, since the values of their two oxidation peak currents are close to those of their two reduction peak currents, the two irreversible oxidation processes of **5** can be attributed to the two sequential one-electron oxidation processes of the two iron atoms attached to the diisonitrile ligand: $Fe^IFe^I(CNC_6H_4) \rightarrow Fe^IFe^{II}(CNC_6H_4) + e^-$ and $(C_6H_4NC)Fe^IFe^I \rightarrow (C_6H_4NC)Fe^{II}Fe^I + e^-$. Namely, the iron atom that is in the first diiron subsite and attached to the diisonitrile ligand is first oxidized and then the iron atom in the next diiron subsite and attached to the diisonitrile ligand is oxidized.

More interestingly, we further found that **1** has the catalytic ability to reduce the protons of acetic acid, a weak acid, to give hydrogen under electrochemical conditions. This catalytic behavior was studied by cyclic voltammetry in the presence of HOAc (0−10 mM) in MeCN (Figure 12). When the first 2 mM of acetic acid was added, the current intensity of the initial first reduction peak at −1.59 V was slightly increased but did not continue to grow with sequential increments of the acid. However, in contrast to this, when the first 2 mM of the acid was added, the initial second reduction at −2.10 V shifted slightly negatively and the current

(27) Gloaguen, F.; Lawrence, J. D.; Rauchfuss, T. B. *J. Am. Chem. Soc.* **2001**, *123*, 9476.
(28) Mejia-Rodriguez, R.; Chong, D.; Reibenspies, J. H.; Soriaga, M. P.; Darensbourg, M. Y. *J. Am. Chem. Soc.* **2004**, *126*, 12004.
(29) Borg, S. J.; Behrsing, T.; Best, S. P.; Razavet, M.; Liu, X.; Pickett, C. J. *J. Am. Chem. Soc.* **2004**, *126*, 16988.
(30) Ott, S.; Kritikos, M.; Åkermark, B.; Sun, L.; Lomoth, R. *Angew. Chem., Int. Ed.* **2004**, *43*, 1006.
(31) Liu, T.; Wang, M.; Shi, Z.; Cui, H.; Dong, W.; Chen, J.; Åkermark, B.; Sun, L. *Chem. Eur. J.* **2004**, *10*, 4474.

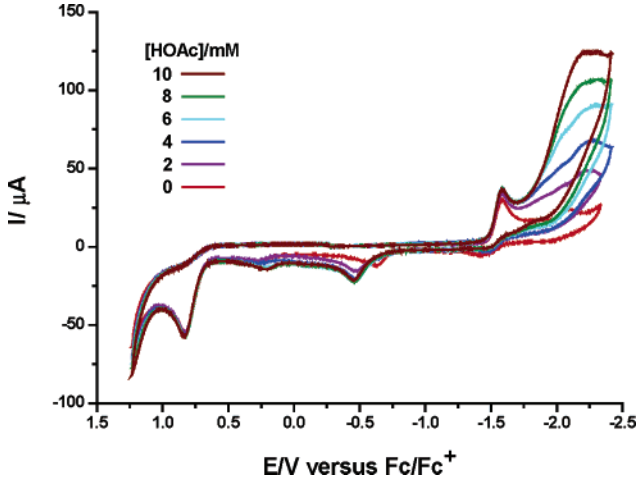

Figure 12. Cyclic voltammgrams of **1** (1 mM) with HOAc (0, 2, 4, 6, 8, 10 mM) in 0.1 M n-Bu_4NPF_6/MeCN at a scan rate of 100 mV·s^{-1}.

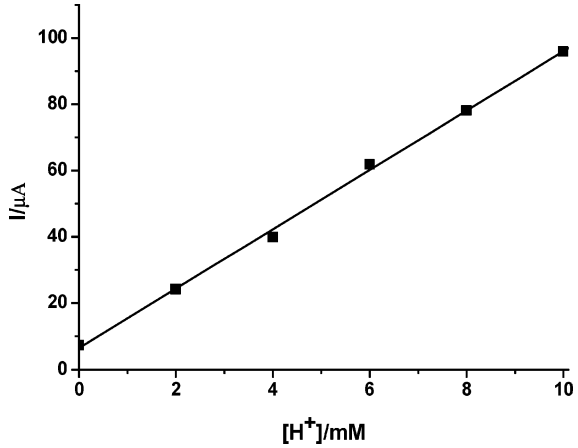

Figure 13. Dependence of current heights of the electrocatalytic peaks of **1** (1 mM) on concentration of HOAc.

intensity of the second reduction continuously increased linearly with increasing concentration of the acid (Figure 13). Such observations are typical of an electrocatalytic proton reduction process. Further evidence for the electrocatalytic activity of **1** was obtained by bulk electrolysis of a MeCN solution of **1** (0.33 mM) with acetic acid (6.6 mM) at −2.16 V, a potential slightly beyond the second reduction peak. The initial rate of the electrolysis is ca. 5 times higher than that in the absence of the catalyst. The rate of electrolysis slowed as the proton concentration decreased, and over the course of 1 h, the total charge passed through the cell approached its maximum, namely 11 F per mol of **1**. This corresponds to 5.5 turnovers. In such a preparative scale experiment, bubbles of H_2 were clearly seen. Gas chromatographic analysis indicated that the hydrogen yield was 100 (±10)%.

Scheme 4 shows the suggested EECC (electrochemical-electrochemical-chemical-chemical) mechanism for this electrocatalytic H_2 production based on similar reported cases[27,31,32] and the electrochemical observations described above. That is, in the presence of acetic acid model compound **1** will first undergo one-electron

Scheme 4[a]

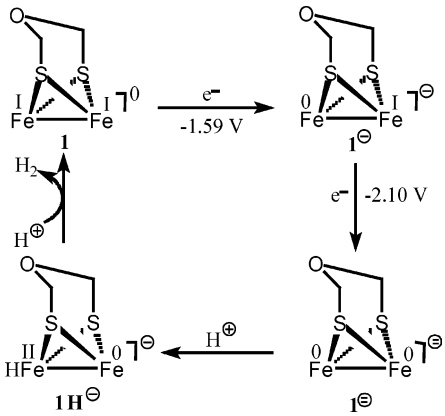

[a] All the carbonyls attached to Fe atoms are omitted for clarity.

reduction at −1.59 V to give intermediate $\mathbf{1}^-$. Further reduction of $\mathbf{1}^-$ at −2.10 V produces intermediate $\mathbf{1}^{2-}$, which is then protonated on its electron-rich Fe core by acetic acid to generate intermediate $\mathbf{1H}^-$. Finally, further protonation of $\mathbf{1H}^-$ yields hydrogen. It is worth pointing out that in the absence of **1** the proton reduction of acetic acid occurred at −2.3 V; thus the electrocatalyst **1** lowers the reduction electropotential of acetic acid up to −0.20 V.

While this mechanism is similar to that proposed for the carbon chain-bridged all-carbonyl diiron complexes,[32] it is different from the CCEE mechanism proposed for the H_2 production from HOTs catalyzed by the PDT type model $[Fe_2(\mu\text{-}SCH_2CH_2CH_2S\text{-}\mu)(CO)_4(CN)(Me_3P)]^-$, in which the electron density at the Fe−Fe bond is remarkably increased by substitution of the strong electron-donating Me_3P and CN^- ligands.[27] It is also different from the CECE mechanism for H_2 production from HOAc catalyzed by the ADT type model $Fe_2(\mu\text{-}SCH_2)_2N(4\text{-}NO_2C_6H_4)(CO)_6$, since in this model the bridged central N atom is first protonated before reduction. In our case, the bridged central oxygen atom in **1** is a weaker Lewis base than the corresponding nitrogen atom in the ADT type model compound,[31] and thus it cannot be protonated before reduction by the weak acid HOAc.

Experimental Section

General Comments. All manipulations were performed using standard Schlenk and vacuum-line techniques under N_2 atmosphere. Dichloromethane was distilled over P_2O_5 under N_2. Acetonitrile was distilled once from P_2O_5 and then freshly distilled from CaH_2 under N_2 before use. Toluene, THF, and hexane were purified by distillation under N_2 from sodium/benzophenone ketyl. $LiBEt_3H$ (1 M in THF), Et_4NCN, $Me_3NO{\cdot}2H_2O$, and Ph_3P were available commercially and used as received. $(\mu\text{-}S_2)Fe_2(CO)_6$,[21a] $(ClCH_2O)_2O$,[33] $Cp(CO)_2FeSPh$,[34] 1,4-diisocyanobenzene,[35] 1,1′-bis(diphenylphosphino)ferrocene,[36] 1,1′-bis(diphenylphosphio)ruthenocene,[37] $[Ph_2PCH_2CH_2OCH_2]_2$,[38] and $[(Ph_2PCH_2)_2NCH_2]_2$[39] were prepared according to literature procedures. Preparative TLC was carried out on glass plates

(32) Chong, D.; Georgakaki, I. P.; Mejia-Rodriguez, R.; Sanabria-Chinchilla, J.; Soriaga, M. P.; Darensbourg, M. Y. *Dalton Trans*. **2003**, 4158.

(33) Buc, S. R. *Org. Synth.* **1956**, *36*, 1.

(34) Ahamad, M.; Bruce, R.; Knox, G. R. *J. Organomet. Chem.* **1966**, *6*, 1.

(35) Efraty, A.; Feinstein, I.; Wackerle, L.; Goldman, A. *J. Org. Chem.* **1980**, *45*, 4059.

(36) Bishop, J. J.; Davison, A.; Katcher, M. L.; Lichtenberg, D. W.; Merril, R. E.; Smart, J. C. *J. Organomet. Chem.* **1971**, *27*, 241.

(26 × 20 × 0.25 cm) coated with silica gel H (10−40 μm). IR spectra were recorded on a Bruker Vector 22 infrared spectrophotometer. ^{1}H (^{31}P) NMR were recorded on a Bruker AC-P 200 NMR spectrometer. Elemental analyses were performed on an Elementar Vario EL analyzer. Melting points were determined on a Yanaco MP-500 apparatus and were uncorrected.

Preparation of $Fe_2(\mu\text{-}SCH_2OCH_2S\text{-}\mu)(CO)_6$ (1). Method i: A solution of $(\mu\text{-}S_2)Fe_2(CO)_6$ (0.172 g, 0.50 mmol) in THF (20 mL) was cooled to −78 °C by a dry ice/acetone bath. To this solution was added Et_3BHLi (1.0 mL, 1.0 mmol) by syringe. At the midpoint of the addition the reaction solution turned from red to a dark emerald green; for the rest of the addition it remained green. To this green solution was added (at −78 °C) bischloromethyl ether (0.173 g, 1.50 mmol), and the color changed back to red. The dry ice/acetone bath was removed, and the red mixture was stirred for 3 h at room temperature. Solvent was removed in vacuo, and the residue was subjected to TLC using CH_2Cl_2/petroleum ether (1:4 v/v) as eluent. From the main orange-red band, **1** (0.117 g, 60%) was obtained as a red solid, mp 110−112 °C. Anal. Calcd for $C_8H_4Fe_2O_7S_2$: C, 24.77; H, 1.04. Found: C, 24.32; H, 1.51. IR (KBr disk): $\nu_{C\equiv O}$ 2077 (s), 2035 (vs), 2002 (vs), 1989 (vs) cm^{-1}. ^{1}H NMR (200 MHz, $CDCl_3$): 4.21 (s, 4H, $2CH_2$) ppm. Method ii: A solution of $(\mu\text{-}S_2)Fe_2(CO)_6$ (0.688 g, 2.0 mmol) in THF (30 mL) was cooled to −78 °C, and then Et_3BHLi (4.0 mL, 4.0 mmol) was added. After the mixture was stirred at this temperature for 15 min, trifluoroacetic acid (0.32 mL, 4.3 mmol) was added, and this mixture was stirred for an additional 10 min. Then bischloromethyl ether (0.450 g, 3.0 mmol) and triethylamine (1.12 mL, 8.0 mmol) were added and stirred for 30 min at −78 °C and for 4 h at room temperature. The same workup as for method i afforded **1** (0.200 g, 26%).

Preparation of $[Fe_2(\mu\text{-}SCH_2OCH_2S\text{-}\mu)(CN)(CO)_5](Et_4N)$ (2). To the red solution of **1** (0.194 g, 0.50 mmol) in MeCN (15 mL) was added a solution of $Me_3NO{\cdot}2H_2O$ (0.056 g, 0.50 mmol) in MeCN (10 mL) at room temperature. The mixture was stirred at this temperature for 10−15 min and then cooled to ca. −40 °C. To this cooled mixture was added a solution of Et_4NCN (0.078 g, 0.50 mmol) in MeCN (10 mL). After 0.5 h, the mixture was allowed to warm to room temperature and stirred for an additional 1 h. After removal of solvent, the residue was throughly washed with CH_2Cl_2/Et_2O (1:5 v/v) and hexane, respectively. **2** (0.160 g, 62%) was obtained as a red solid, mp 106 °C (dec). Anal. Calcd for $C_{16}H_{24}Fe_2N_2O_6S_2$: C, 37.22; H, 4.69. N, 5.42. Found: C, 37.10; H, 4.62; N, 5.49. IR (KBr disk): $\nu_{C\equiv N}$ 2088 (s); $\nu_{C\equiv O}$ 2030 (vs), 1987 (vs), 1968 (vs), 1945 (s), 1907 (vs) cm^{-1}. ^{1}H NMR (200 MHz, $CDCl_3$): 4.09 (s, 4H, $2SCH_2$), 3.31 (q, J = 6.2 Hz, 8H, $4CH_2CH_3$), 1.34 (br s, 12H, $4CH_2CH_3$) ppm.

Preparation of $Fe_2(\mu\text{-}SCH_2OCH_2S\text{-}\mu)(CO)_5(PPh_3)$ (3). A solution of $Me_3NO{\cdot}2H_2O$ (0.056 g, 0.50 mmol) in MeCN (10 mL) at room temperature was added to a solution of **1** (0.194 g, 0.50 mmol) and PPh_3 (0.131 g, 0.50 mmol) in MeCN (15 mL). The mixture was stirred at this temperature for 1 h. Solvent was removed, and the residue was subjected to TLC using CH_2Cl_2/petroleum ether (1:3 v/v) as eluent. From the main red band, **3** (0.290 g, 93%) was obtained as a red solid, mp 204−205 °C. Anal. Calcd for $C_{25}H_{19}Fe_2O_6PS_2$: C, 48.26; H, 3.08. Found: C, 47.98; H, 3.07. IR (KBr disk): $\nu_{C\equiv O}$ 2041 (vs), 1978 (vs), 1957 (vs), 1935 (s) cm^{-1}. ^{1}H NMR (200 MHz, $CDCl_3$): 7.71, 7.42 (2 br s, 15H, $3C_6H_5$), 3.74 (br s, 2H, $2CHOCH$), 3.38 (br s, 2H, $2CHOCH$). ^{31}P NMR (81.0 MHz, $CDCl_3$, H_3PO_4): 63.93 (s) ppm.

Preparation of $[Fe_2(\mu\text{-}SCH_2OCH_2S\text{-}\mu)(CO)_5][Cp(CO)_2FeSPh]$ (4). A solution of **1** (0.194 g, 0.50 mmol) in MeCN (15 mL) was treated with a solution of $Me_3NO{\cdot}2H_2O$ (0.056 g, 0.50 mmol) in MeCN (10 mL) at room temperature for 10−15 min. To this mixture was added a solution of $Cp(CO)_2FeSPh$ (0.143 g, 0.50 mmol) in MeCN (10 mL), and then the mixture was stirred for 1 h. After removal of solvent, the residue was subjected to TLC by using Et_2O/petroleum ether (1:1 v/v) as eluent to give **4** as a brown-red solid (0.233 g, 72%), mp 114−116 °C. Anal. Calcd for $C_{20}H_{14}Fe_3O_8S_3$: C, 37.18; H, 2.18. Found: C, 37.23; H, 2.23. IR (KBr disk): $\nu_{C\equiv O}$ 2034 (vs), 1992 (vs), 1974 (vs), 1964 (s), 1914 (s) cm^{-1}. ^{1}H NMR (200 MHz, $CDCl_3$): δ 7.19−7.68 (m, 5H, C_6H_5), 4.99 (s, 5H, C_5H_5), 4.14 (br s, 2H, $2CHOCH$), 3.90 (br s, 2H, $2CHOCH$) ppm.

Preparation of $[Fe_2(\mu\text{-}SCH_2OCH_2S\text{-}\mu)(CO)_5]_2[1,4\text{-}(CN)_2C_6H_4]$ (5). To the red solution of **1** (0.194 g, 0.50 mmol) in CH_2Cl_2/MeCN (15 mL) (1:2 v/v) were successively added a solution of $Me_3NO{\cdot}2H_2O$ (0.056 g, 0.50 mmol) in MeCN (15 mL) and a solution of 1,4-diisocyanobenzene (0.032 g, 0.25 mmol) in CH_2Cl_2 (10 mL). The mixture was stirred at room temperaure for 1 h. The same workup as for **3** afforded **5** (0.120 g, 57%) as a red solid, mp 176 °C (dec). Anal. Calcd for $C_{22}H_{12}Fe_4N_2O_{12}S_4$: C, 31.16; H, 1.43; N, 3.30. Found: C, 31.23; H, 1.47; N, 3.20. IR (KBr disk): $\nu_{N=C}$ 2121 (vs); $\nu_{C\equiv O}$ 2040 (s), 2010 (vs), 1971 (vs) cm^{-1}. ^{1}H NMR (200 MHz, $CDCl_3$): 7.28 (s, 4H, C_6H_4), 4.19 (s, 8H, $4SCH_2$) ppm.

Preparation of $[Fe_2(\mu\text{-}SCH_2OCH_2S\text{-}\mu)(CO)_5]_2[(\eta^5\text{-}Ph_2PC_5H_4)_2Fe]$ (6). A solution of **1** (0.194 g, 0.50 mmol) in MeCN (15 mL) was treated with a solution of $Me_3NO{\cdot}2H_2O$ (0.056 g, 0.50 mmol) in MeCN (10 mL) at room temperature. The mixture was stirred for 20 min, and then to this mixture was added $(\eta^5\text{-}Ph_2PC_5H_4)_2Fe$ (dppf) (0.139 g, 0.25 mmol). The new mixture was stirred at room temperature for 4 h. After solvent removal, the residue was subjected to TLC using petroleum ether/acetone (4:1 v/v) as eluent to give **6** as a red solid (0.288 g, 90%), mp 171 °C (dec). Anal. Calcd for $C_{48}H_{36}Fe_5O_{12}P_2S_4$: C, 45.25; H, 2.85. Found: C, 45.45; H, 3.01. IR (KBr disk): $\nu_{C\equiv O}$ 2047 (vs), 1983 (vs), 1933 (s) cm^{-1}. ^{1}H NMR (200 MHz, $CDCl_3$): δ 7.38−7.60 (m, 20H, $4C_6H_5$), 4.25 (d, 8H, $2C_5H_4$), 3.50, 3.65 (2d, 8H, $4SCH_2$) ppm. ^{31}P NMR (81.0 MHz, $CDCl_3$, H_3PO_4): 54.16 (s) ppm.

Preparation of $[Fe_2(\mu\text{-}SCH_2OCH_2S\text{-}\mu)(CO)_5]_2[(\eta^5\text{-}Ph_2PC_5H_4)_2Ru]$ (7). The same procedure was followed as for **6**, but $(\eta^5\text{-}Ph_2PC_5H_4)_2Ru$ (dppr) (0.150 g, 0.25 mmol) was used. **7** (0.278 g, 84%) was obtained as a red solid, mp 192 °C (dec). Anal. Calcd for $C_{48}H_{36}Fe_4O_{12}P_2RuS_4$: C, 43.67; H, 2.73. Found: C, 43.63; H, 2.75. IR (KBr disk): $\nu_{C\equiv O}$ 2047 (vs), 1984 (vs), 1935 (s) cm^{-1}. ^{1}H NMR (200 MHz, $CDCl_3$): 7.36−7.62 (m, 20H, $4C_6H_5$), 4.56 (d, 8H, $2C_5H_4$), 3.54, 3.68 (2d, 8H, $4SCH_2$) ppm. ^{31}P NMR (81.0 MHz, $CDCl_3$, H_3PO_4): 53.63 (s) ppm.

Preparation of $[Fe_2(\mu\text{-}SCH_2OCH_2S\text{-}\mu)(CO)_5]_2\text{-}(Ph_2PCH_2CH_2OCH_2)_2$ (8). To a solution of **1** (0.194 g, 0.50 mmol) in toluene (20 mL) was added $(Ph_2PCH_2CH_2OCH_2)_2$ (0.123 g, 0.25 mmol). The mixture was stirred at reflux for 2 h. After removal of solvent at reduced pressure, the residue was subjected to TLC using petroleum ether/Et_2O (5:2 v/v) as eluent to give **8** as a red solid (0.260 g, 86%), mp 146 °C (dec). Anal. Calcd for $C_{44}H_{40}Fe_4O_{14}P_2S_4$: C, 43.78; H, 3.32. Found: C, 43.61; H, 3.29. IR (KBr disk): $\nu_{C\equiv O}$ 2047 (vs), 1981 (vs), 1933 (s) cm^{-1}. ^{1}H NMR (200 MHz, $CDCl_3$): 7.39−7.72 (m, 20H, $4C_6H_5$), 3.63−3.75 (m, 12H, $4SCH_2$, $2PCH_2CH_2O$), 3.40 (s, 4H, OCH_2CH_2O), 2.75−2.90(m, 4H, $2PCH_2$) ppm. ^{31}P NMR (81.0 MHz, $CDCl_3$, H_3PO_4): 48.09 (s) ppm.

Preparation of $[Fe_2(\mu\text{-}SCH_2OCH_2S\text{-}\mu)(CO)_4]_2\text{-}[(Ph_2PCH_2)_2NCH_2]_2$ (9). The same procedure was followed as for **8**, but $[(Ph_2PCH_2)_2NCH_2]_2$ (0.223 g 0.25 mmol) and the eluent of petroleum ether/CH_2Cl_2 (5:3 v/v) were employed. **9** (0.213 g, 56%) was obtained as a red solid, mp 183 °C (dec). Anal. Calcd for $C_{66}H_{60}Fe_4N_2O_{10}P_4S_4$: C, 52.27; H, 3.99; N, 1.85. Found: C, 51.99; H, 3.91, N, 2.03. IR (KBr disk): $\nu_{C\equiv O}$ 2023 (vs), 1949 (vs), 1900 (s) cm^{-1}. ^{1}H NMR (200 MHz, $CDCl_3$): δ 7.10−7.68 (m, 40H, $8C_6H_5$), 3.88−3.24 (m, 16H, $4SCH_2$, 4

(37) Li, S.; Wei, B.; Low, P. M. N.; Lee, H. K.; Andy Hor, T. S.; Xue, F.; Mak, T. C. W. *J. Chem. Soc., Dalton Trans.* **1997**, 1289.
(38) Heuer, B.; Pope, S. J. A.; Reid, G. *Polyhedron* **2000**, *19*, 743.
(39) Grim, S. O.; Matienzo, L. J. *Tetrahedron Lett.* **1973**, 2951.

Table 3. Crystal Data and Structural Refinement Details for 1, 2, 4, and 5

	1	2	4	5
mol formula	$C_8H_4Fe_2O_7S_2$	$C_{16}H_{24}Fe_2N_2O_6S_2$	$C_{20}H_{14}Fe_3O_8S_3$	$C_{22}H_{12}Fe_4N_2O_{12}S_4$
mol wt	387.93	516.19	646.04	847.98
cryst syst	monoclinic	monoclinic	orthorhombic	monoclinic
space group	*P*2(1)/*m*	*C*2/*c*	P2(1)2(1)2(1)	*C*2/*c*
a/Å	6.833 (3)	32.554(12)	11.021(7)	29.406(13)
b/Å	13.633(6)	11.294(4)	13.173(8)	7.598(3)
c/Å	7.711(3)	13.655(5)	16.851(10)	15.657(7)
α/deg	90	90	90	90
β/deg	109.421(6)	114.653(11)	90	113.949(7)
γ/deg	90	90	90	90
V/Å^3	677.4(5)	4563(3)	2446(2)	3088(2)
Z	2	8	4	4
D_c/g·cm^{-3}	1.902	1.503	1.754	1.824
abs coeff/mm^{-1}	2.470	1.486	2.055	2.173
F(000)	384	2128	1296	1688
$2\theta_{max}$/deg	52.70	50.10	52.88	54.82
no. of reflns	3205	11 336	14 551	8628
no. of indep reflns	1442	3992	5025	3171
index ranges	$-3 \le h \le 8$ $-16 \le k \le 11$ $-9 \le l \le 8$	$-38 \le h \le 37$ $-13 \le k \le 11$ $-15 \le l \le 16$	$-13 \le h \le 13$ $-16 \le k \le 8$ $-20 \le l \le 20$	$-25 \le h \le 35$ $-8 \le k \le 9$ $-18 \le l \le 19$
goodness of fit	1.012	1.009	0.974	1.029
R	0.0324	0.0552	0.0362	0.0354
R_w	0.0605	0.1071	0.0599	0.0794
largest diff peak and hole/e Å^{-3}	0.405/−0.299	0.821/−0.335	0.346/−0.358	0.7006/−0.292

Table 4. Crystal Data and Structural Refinement Details for 6−9

	6	7	8	9
mol formula	$C_{48}H_{36}Fe_5O_{12}P_2S_4 \cdot 3CH_2Cl_2$	$C_{48}H_{36}Fe_4O_{12}P_2RuS_4 \cdot 2PhCl$	$C_{44}H_{40}Fe_{24}O_{14}P_2S_4$	$C_{66}H_{60}Fe_4N_2O_{10}P_4S_4 \cdot 2PhCl \cdot 2CH_2Cl_2$
mol wt	1528.98	1544.52	1206.34	1911.64
cryst syst	triclinic	monoclinic	monoclinic	triclinic
space group	$P\bar{1}$	*C*2/*c*	*P*2(1)/*n*	$P\bar{1}$
a/Å	10.422(6)	33.484(12)	15.931(9)	11.244(6)
b/Å	13.454(6)	9.174(3)	18.653(11)	13.596(7)
c/Å	14.360(8)	21.475(8)	17.065(10)	15.158(7)
α/deg	117.430(12)	90	90	76.821(9)
β/deg	106.307(10)	109.0645	101.361(10)	72.850(9)
γ/deg	94.840(10)	90	90	81.230(8)
V/Å^3	1660.4(14)	6235(4)	4972(5)	2146.9(19)
Z	1	4	4	2
D_c/g·cm^{-3}	1.529	1.645	1.612	1.479
abs coeff/mm^{-1}	1.534	1.476	1.440	1.077
F(000)	770	3112	2456	978
$2\theta_{max}$/deg	53.08	52.80	50.00	53.28
no. of reflns	9482	17 329	25 217	12 458
no. of indep reflns	6645	6373	8746	8812
index ranges	$-12 \le h \le 13$ $-16 \le k \le 8$ $-14 \le l \le 17$	$-41 \le h \le 41$ $-11 \le k \le 10$ $-26 \le l \le 23$	$-16 \le h \le 18$ $-22 \le k \le 12$ $-20 \le l \le 20$	$-14 \le h \le 12$ $-17 \le k \le 17$ $-19 \le l \le 8$
goodness of fit	1.015	1.172	1.040	1.034
R	0.0576	0.0496	0.0649	0.0675
R_w	0.1432	0.1063	0.1449	0.1500
largest diff peak and hole/e Å^{-3}	0.738/−0.624	0.860/−0.551	0.744/−0.530	0.937/−0.688

PCH_2), 2.24 (s, 4H, $2NCH_2$) ppm. ^{31}P NMR (81.0 MHz, $CDCl_3$, H_3PO_4): δ 54.32 (s) ppm.

X-ray Structure Determination of 1, 2, and 4−9. Single crystals of **1**, **2**, and **4**−**9** suitable for X-ray diffraction analyses were grown by slow evaperation of their haxane solution at about 4 °C. Each single crystal was mounted on a Bruker SMART 1000 automated diffractometer, respectively. Data were collected at room temperature, using graphite-monochromated Mo Kα radiation (λ = 0.71073 Å) in the ω−2θ scanning mode. Absorption corrections were performed using SADABS. The structures were solved by direct methods using the SHELXS-97 program[40] and refined by full-matrix least-squares techniques (SHELXL-97)[41] on F^2. Hydrogen atoms were located by using the geometric method. Details of crystal data, data collections, and structure refinements are summarized in Tables 3 and 4, respectively.

Electrochemistry. Acetonitrile (Fisher Chemicals, HPLC grade) for electrochemistry assays was used directly without further purification. A solution of 0.1 M *n*-Bu_4NPF_6 in CH_3CN was used as electrolyte in all cyclic voltammetric experiments. The electrolyte solution was degassed by bubbling with dry N_2 for 10 min before measurement. Electrochemical measurements were made using a BAS Epsilon potentiostat. All voltammograms were obtained in a three-electrode cell with a 3 mm diameter glassy carbon working, platinum counter, and Ag/Ag^+ (0.01 M $AgNO_3$/0.1 M *n*-Bu_4NPF_6 in CH_3-

(40) Sheldrick, G. M. *SHELXS97*, A Program for Crystal Structure Solution; University of Göttingen: Germany, 1997.

(41) Sheldrick, G. M. *SHELXL97*, A Program for Crystal Structure Refinement; University of Göttingen: Germany, 1997.

CN) reference electrode under N_2 atmosphere. The working electrode was polished with 1 μm diamond paste and sonicated in water for 10 min prior to use. All potentials are quoted against the ferrocene/ferrocenium (Fc/Fc^+) potential. Bulk electrolyses for electrocatalytic reactions were carried out under N_2 atmosphere using a BAS Epsilon potentiostat. Electrocatalytic experiments were run on a glassy carbon rod ($A = 2.9$ cm^2) in a two-compartment, gastight, H-type electrolysis cell containing ca. 25 mL of CH_3CN. The electrolyses of solutions were carried out under hydrodynamic conditions, vigorously stirring the solutions, to mitigate mass transport complications. Gas chromatography was performed with a Shimadzu gas chromatograph GC-9A under isothermal conditions with nitrogen as a carrier gas and a thermal conductivity detector.

Acknowledgment. We are grateful to the National Natural Science Foundation of China, the State Key Laboratory of Organometallic Chemistry, and the Specialized Research Fund for the Doctoral Program of Higher Education of China for financial support of this work.

Supporting Information Available: Full tables of crystal data, atomic coordinates and thermal parameters, and bond lengths and angles for **1**, **2**, and **4**−**9** as CIF files. This material is available free of charge via the Internet at http://pubs.acs.org.

OM0507373